Hindawi
Journal of Sensors
Volume 2021, Article ID 1565567, 14 pages
https://doi.org/10.1155/2021/1565567

Research Article

Accurate and Contactless Vital Sign Detection in Short Time Window with 24 GHz Doppler Radar

Yu Xu, Qi Li, and Zhenzhou Tang

College of Computer and Artificial Intelligence, Wenzhou University, Wenzhou 325035, China

Correspondence should be addressed to Yu Xu; yxu@wzu.edu.cn

Received 3 June 2021; Revised 8 August 2021; Accepted 18 September 2021; Published 5 October 2021

Academic Editor: Jerome Rossignol

Breathing and heartbeat are critical vital signs which reflect the health status of human beings. Aiming to accurately measure the vital sign in short time window, a novel signal processing method for Doppler radar vital sign detection is proposed. Firstly, a two-step I/Q mismatch correction method which, respectively, estimates the time invariant phase imbalance and gain ratio of I/Q channels in the calibration step and the direct-current offsets during normal operation has been proposed. By decreasing the number of estimation parameters from 5 to 2, the parameters can be effectively estimated with data distributed over shorter arc lengths. Then, to solve the discontinuity occurred in arctangent demodulation, the displacement information of chest movement is extracted from the calibrated I/Q signals by extended differentiate and cross multiply algorithm. Finally, instead of Fourier transform-based methods which require long time windows to guarantee sufficient frequency resolution, the optimal parameters of respiration and heartbeat are found by the intelligent search of the differential evolution algorithm. The experimental results show that the proposed method can accurately measure respiratory rate and heartbeat rate with a short time window. For the 8 s time window, the mean absolute errors of respiration and heartbeat were 0.52 bpm and 0.79 bpm, respectively, demonstrating its promise in real-time applications.

1. Introduction

Breathing and heartbeat are important vital signs as well as key indicators of health condition, sleep quality [1–3], etc. Most physiological diseases and physical abnormalities usually lead to changes in respiration and heartbeat. Therefore, continuous and accurate monitoring of respiration and heartbeat in daily life is very critical for early diagnosis of disease.

Polysomnography (PSG) [4] is the primary clinical tool for monitoring respiration and heartbeat. However, PSG is usually limited to clinical usage due to the professional installation of electrodes and expensive monitors. Sensors such as thermistor [5], magnetometer [6], accelerometer [7, 8], and gyroscope [9] have also been utilized to provide ubiquitous low-cost vital sign monitoring by detecting the temperature change in the nasal cavity [5] or the chest wall motion [6–9]. However, these sensors need to be in close contact with the human body, which will inevitably cause discomfort. In order to avoid the discomfort, some noncontact approaches using the monocular camera [10], the depth camera [11], the received signal strength of ZigBee [12], the channel state information of Wi-Fi [13], the ultrawideband (UWB) radar [14], and the continuous wave (CW) Doppler radar [15–17] have been proposed. Among them, the continuous wave Doppler radar working at higher frequency has attracted the attention of researchers due to its merits of high sensitivity, antijamming performance, and simple radio frequency circuit structure.

The signal processing of Doppler radar-based vital sign detection is regarded as a baseband phase demodulation problem [18]. Small angle approximation method [19] can be used to extract vital signs when the amplitude of chest movement is much smaller than the carrier wavelength of radar. However, for high frequency radar with short wavelength, the problems of null detection [19] and small-angle limitation [20] are inevitable. The complex signal demodulation technique [21, 22] was proposed for solving the null

detection problem reliably with a quadrature receiver. However, the measurement of heartbeat can be easily affected by the interference of respiration. To reduce the interference of respiratory harmonics, a long time window is required to obtain a sufficient frequency spectrum solution [23]. To overcome the limitation of small angle approximation, the arctangent demodulation [24, 25] was proposed. However, it relies on accurate direct-current offset compensation and quadrature channel imbalance elimination. Besides, the extended differentiate and cross multiply algorithm was proposed [26] to solve the phase entanglement problem in arctangent demodulation. The abovementioned methods usually use fast Fourier transform (FFT) to extract the frequency of breathing and heartbeat. However, as the frequency resolution of FFT is inversely proportional to the time window, the time window must be increased to improve the measurement accuracy, which leads to the degradation of real-time performance.

In order to avoid the frequency resolution problem of FFT and improve the real-time performance, we propose a novel signal processing method for Doppler radar vital sign detection. The main contribution of this paper is as follows.

(1) To effectively estimate and compensate the radar imbalance from data distributed over short arc length, a two-step correction method has been proposed. Since the phase imbalance and the gain ratio of I/Q channels are time invariant, we only estimate them in the calibration step and treat them as constants in normal operation. As a result, only direct-current offsets of I/Q channels need to be estimated in normal operation, which effectively reduce the requirement of arc length

(2) To accurately measure vital signs with data in short time window, the phase demodulation is regarded as a parameter optimization problem, and the vital sign parameters which best fit the displacement of chest movement extracted from the calibrated I/Q signals can be estimated by the differential evolution algorithm. Therefore, the frequency resolution problem of FFT-based methods [21, 27] can be avoided, and the respiratory and heartbeat parameters can be accurately estimated with limited data of short time window

(3) We conducted extensive experiments in real environments and compared them with state-of-the-arts to evaluate the performance of the proposed method. The experimental results show that the proposed approach can achieve accurate and robust vital sign measurement with a limited data length from 24 GHz Doppler radar

The rest of the paper is organized as follows. Section 2 describes the I/Q mismatch correction and displacement signal extraction method in detail. In Section 3, the respiratory and heartbeat parameter extraction method based on the differential evolution algorithm is presented. The experiments and results are given in Section 4, and Section 5 concludes the work.

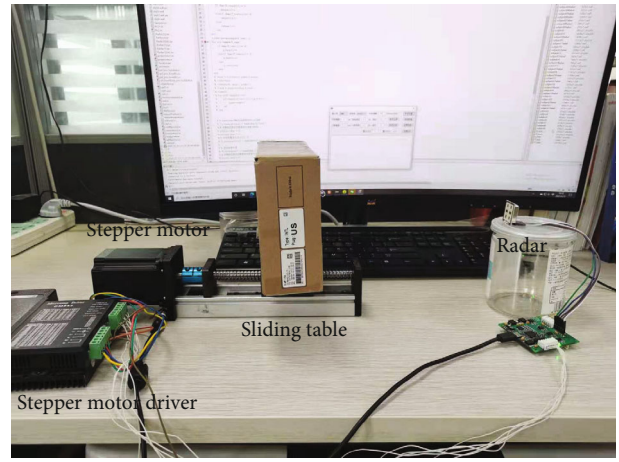

Figure 1: Experimental setup for mechanical motion detection.

2. Signal Preprocessing

2.1. I/Q Mismatch Correction. Ideally, the locus of error-free measurements from the I/Q channels of Doppler radar is a circle centered at the origin. However, the shape of an ideal circle can be easily altered by errors in practice [28].

$$I(t) = A_I \times \cos\left[\frac{4\pi x(t)}{\lambda} + \theta\right] + \mathrm{DC}_I,$$
$$Q(t) = A_Q \times \sin\left[\frac{4\pi x(t)}{\lambda} + \theta + \phi(t)\right] + \mathrm{DC}_Q, \quad (1)$$

where $\theta = 4\pi d_0/\lambda + \theta_0$ is a constant phase shift determined by the initial phase shift θ_0 and the distance d_0 between the radar and the target object. A_I and A_Q are the amplitude of two orthogonal output signals. $x(t)$ is the chest wall displacement due to respiration and heartbeat. λ is the carrier wavelength. DC_I and DC_Q are the direct-current offsets in I/Q channels. $\phi(t)$ is the total residual phase error.

In order to observe the variation of radar error parameters, the hardware-in-the-loop simulation setup shown in Figure 1 is developed to simulate chest wall movement and collect I/Q signals of Doppler radar. Table 1 describes the simulation setup's components. A carton with a size of 10 cm × 10 cm is installed on the sliding table to provide a reflective surface. The sliding table is driven by a stepper motor that is controlled by a microcontroller simulating the chest wall movement. To improve the accuracy of parameter estimation, the displacement of the sliding table is set to ±6 mm to make the collected data distributed on the whole ellipse. Different obstructions such as box, glass, and cloth are placed between the radar and the measured object. A set of radar parameters are estimated by the least square-based ellipse fitting algorithm [29–31] from collected data of I/Q signals under different distances and obstructions. As can be seen from Table 2, the direct-current offsets and the amplitudes vary greatly with

Table 1: Description of the simulation setup's components.

Component	Model	Description
Radar	K-LC5	24 GHz Doppler radar transceiver with I/Q IF outputs
Sliding table	SGX1204-100	Ball screw rail sliding table with screw diameter of 12 mm, screw pitch of 4 mm, and maximum movement distance of 100 mm
Stepper motor	BS57HB76-03	Two phase stepper motor with step angle of 1.8°, torque of 1.5 Nm, and maximum speed of 600 rpm
Stepper motor driver	DM542	Pulse controlled stepper motor driver
Microcontroller	STM32F405	168 MHz cortex-M4 CPU with FPU
Power supply	AC-DC power	+24 V 6.75A

Table 2: Calibration parameters of I/Q signals.

Distances	Obstructions	DC_I (10^6)	DC_Q (10^5)	A_I (10^5)	A_Q(10^5)	A_I / A_Q	ϕ(rad)
20	No	1.77	-4.30	0.91	0.71	1.29	-0.36
40	No	1.77	-4.27	0.92	0.69	1.33	-0.32
60	No	1.72	-3.87	0.93	0.73	1.28	-0.40
80	No	1.40	-8.38	3.46	2.76	1.26	-0.40
100	No	1.85	-5.29	3.52	2.90	1.21	-0.33
20	Box	1.76	-1.35	2.04	1.58	1.29	-0.34
40	Box	1.71	-5.93	2.00	1.52	1.31	-0.30
60	Glass	1.82	-4.73	2.01	1.58	1.28	-0.37
80	Glass	1.72	-3.69	0.54	0.39	1.36	-0.28
100	Cloth	1.52	-5.06	0.27	0.21	1.28	-0.31

distances and obstructions, while the total residual phase error and the ratio of amplitudes remain nearly unchanged. In order to reduce the number of parameters to be estimated, a two-step I/Q mismatch correction method, which estimates the invariant parameters in the calibration step and the variant parameters during normal operation, is proposed.

The calibration step only needs to be performed once before the normal operation. The least-based ellipse fitting algorithm [29] is used to estimate the 5 parameters with sufficient data. Then, the time invariant parameters ϕ and A_I / A_Q can be obtained and finally used for I/Q mismatch correction during the normal operation.

Equation (1) can be expressed as

$$\frac{(I - \mathrm{DC}_I)^2}{A_I^2} + \left(\frac{Q - \mathrm{DC}_Q}{A_Q \cos\phi} - \frac{(I - \mathrm{DC}_I)\sin\phi}{A_I \cos\phi}\right)^2 = 1. \quad (2)$$

Substituting the initial values I_0, Q_0 of the I/Q signals collected by radar in Equation (2), we yield

$$\frac{(I_0 - \mathrm{DC}_I)^2}{A_I^2} + \left(\frac{Q_0 - \mathrm{DC}_Q}{A_Q \cos\phi} - \frac{(I_0 - \mathrm{DC}_I)\sin\phi}{A_I \cos\phi}\right)^2 = 1. \quad (3)$$

By subtracting (3) from (2), we obtain

$$\begin{cases} y = a \times c, \\ y = \left(I^2 - I_0^2\right) + \dfrac{A_I^2}{A_Q^2}\left(Q^2 - Q_0^2\right) - \dfrac{2A_I}{A_Q}\sin\phi(IQ - I_0Q_0), \\ a = [2(I - I_0)2(Q - Q_0)], \\ c = \begin{bmatrix} \mathrm{DC}_I - \dfrac{A_I}{A_Q}\sin\phi\mathrm{DC}_Q \\ \dfrac{A_I^2}{A_Q^2}\mathrm{DC}_Q - \dfrac{A_I}{A_Q}\sin\phi\mathrm{DC}_I \end{bmatrix}. \end{cases} \quad (4)$$

Note that ϕ and A_I / A_Q are the invariant parameters estimated in the calibration step. According to Equation (4), the standard recursive least square algorithm can be applied to estimate parameter c from I/Q signals, and then, DC_I and DC_Q can be calculated. Finally, the radar signals can be calibrated by substituting DC_I, DC_I, A_I / A_Q, and ϕ in Equation (1)

$$I^c(t) = A_I \times \cos\left[\frac{4\pi x(t)}{\lambda} + \theta\right] = I(t) - \mathrm{DC}_I,$$

$$Q^c(t) = A_Q \times \sin\left[\frac{4\pi x(t)}{\lambda} + \theta\right] = \frac{Q(t) - \mathrm{DC}_Q - \left(A_I/A_Q\right)I^c(t)\sin\phi(t)}{\cos\phi(t)}. \quad (5)$$

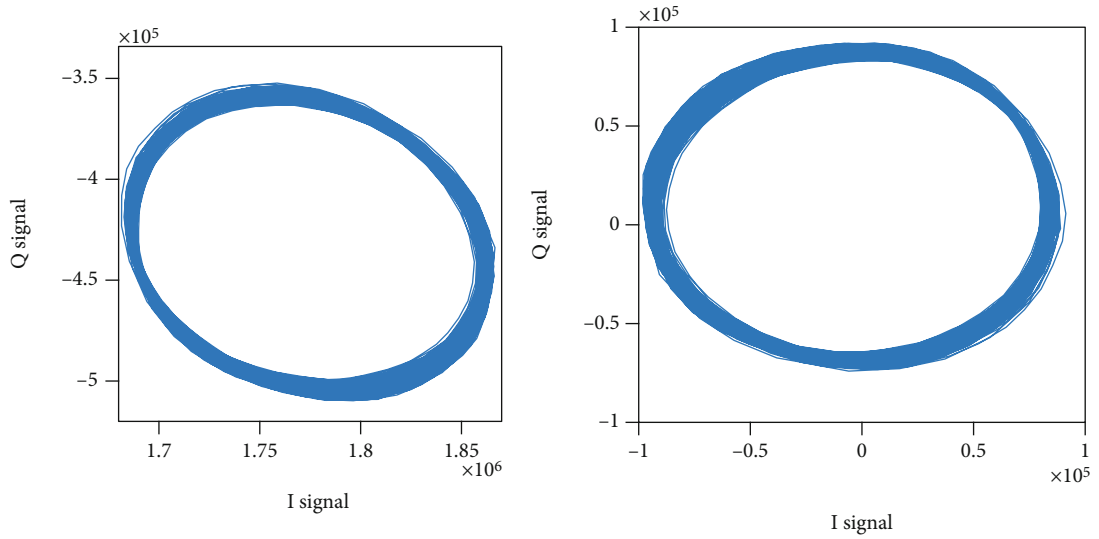

Figure 2: Plan view of I/Q signals after correction: (a) raw I/Q signals; (b) the I/Q signals after eliminating the direct-current offsets and phase error.

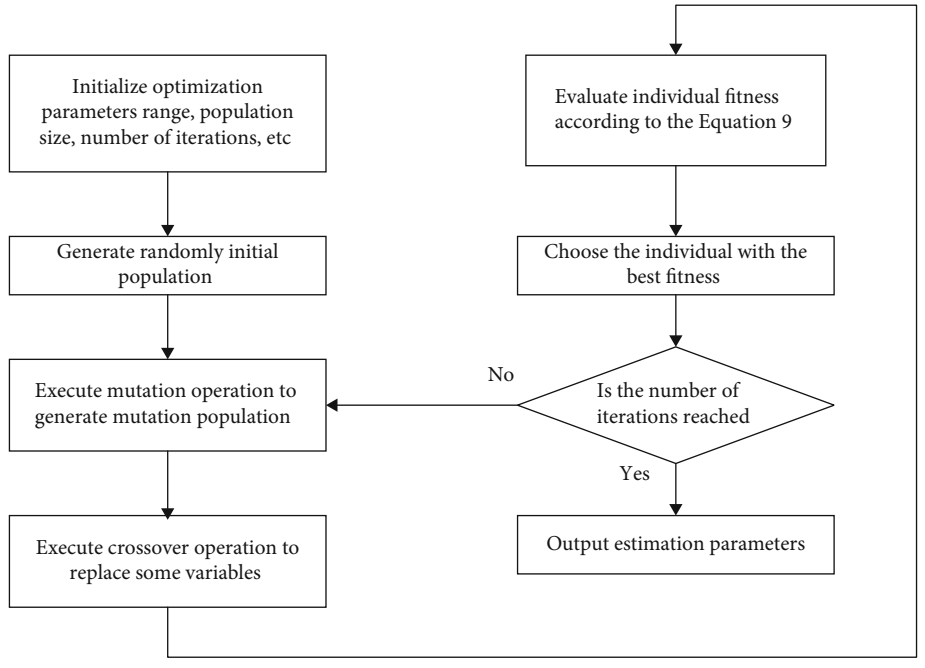

Figure 3: Flow chart of the differential evolution algorithm.

Figure 2 shows the raw and calibrated I/Q signals of radar. As can be seen from Figure 2, the proposed two-step correction method can effectively correct the distorted ellipse into a standard ellipse with center at the origin.

2.2. Displacement Signal Extraction. To solve the discontinuity occurred in the arctangent function when the demodulation exceeds the native codomain range of $(-\pi/2, \pi/2)$, the extended differentiate and cross multiply algorithm [26] is adopted for the demodulation of absolute displacement. The derivative of the displacement information $\dot{x}(t)$ can be expressed as

$$\begin{aligned}\dot{x}(t) &= \frac{\lambda}{4\pi}\frac{d}{dt}\left[\arctan\frac{A_I Q^c(t)}{A_Q I^c(t)}\right] \\ &= \frac{\lambda}{4\pi}\frac{I^c(t)\dot{Q}^c(t) - \dot{I}^c(t)Q^c(t)}{\left(A_Q/A_I\right)I^c(t)^2 + \left(A_I/A_Q\right)Q^c(t)^2},\end{aligned} \tag{6}$$

where $\dot{I}^c(t)$ and $\dot{Q}^c(t)$ are the time derivative of $I^c(t)$ and $Q^c(t)$.

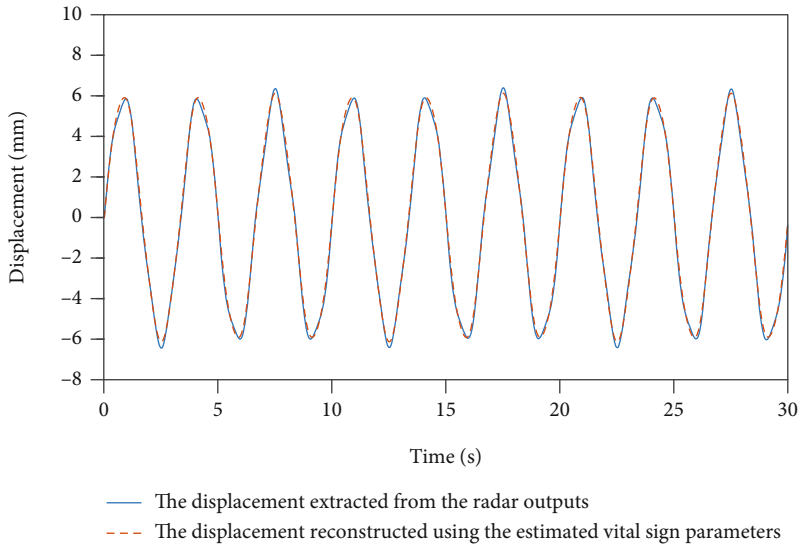

Figure 4: The comparison of the displacement extracted from the radar outputs and the displacement reconstructed using the estimated vital sign parameters.

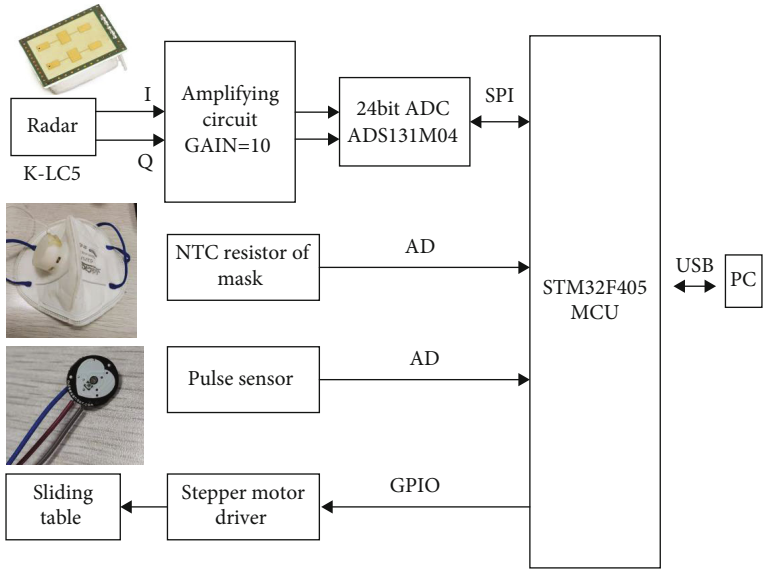

Figure 5: The overall structure of the experimental setup.

Table 3: Displacement MAE under different arc lengths.

Amplitude	Central angle	MAE (percentage of error in displacement)	
		The proposed method	Ellipse fitting algorithm
3 mm	1.92π	0.3049 mm (5.08%)	0.3891 mm (6.49%)
2.5 mm	1.6π	0.2044 mm (4.09%)	0.2938 mm (5.88%)
2 mm	1.28π	0.1944 mm (4.86%)	0.1955 mm (4.89%)
1.5 mm	0.96π	0.1502 mm (5.01%)	0.3293 mm (10.98%)
1 mm	0.64π	0.0827 mm (4.14%)	0.1902 mm (9.51%)
0.5 mm	0.32π	0.1008 mm (11.08%)	2.5702 mm (257.02%)

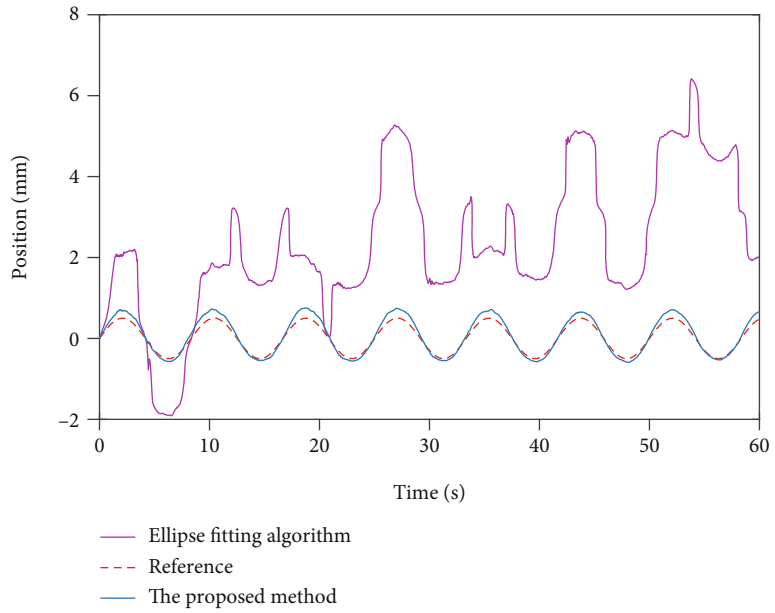

Figure 6: A comparison of the estimated displacement by the proposed method and the ellipse fitting algorithm, when the amplitude is 0.5 mm.

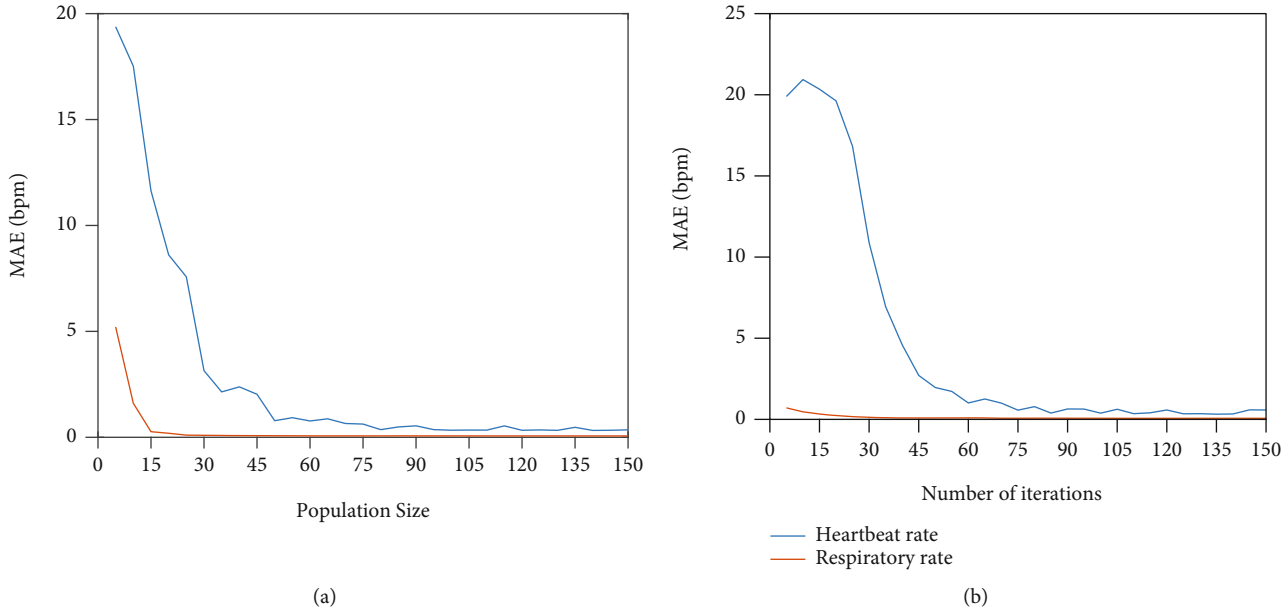

Figure 7: The MAE of estimated respiratory and heartbeat rate with different population sizes and numbers of iterations: (a) the MAE with different population sizes (the number of iterations is set to 100); (b) the MAE with the different numbers of iterations (the population size is set to 80).

Table 4: The parameters for experiments in a controlled environment.

Data	m_r (mm)	f_r (bpm)	φ_r (°)	m_h (mm)	f_h (mm)	φ_h (°)
1	1	12	0	0.1	60	10
2	2	12	0	0.2	60	10
3	3	18	0	0.3	72	20
4	4	24	0	0.4	84	30
5	5	30	0	0.5	96	40
6	6	36	0	0.6	108	50

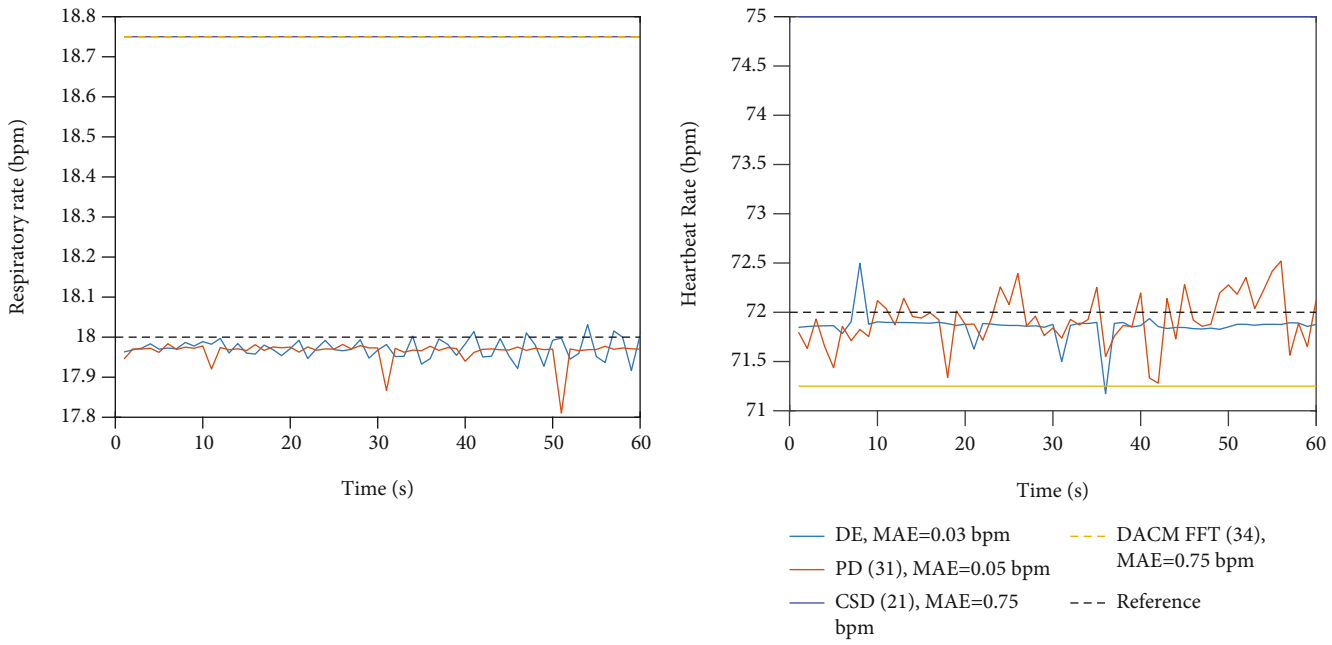

Figure 8: A comparison of estimated respiratory rate and heartbeat rate from data 3 (the sliding window and step size are 16 s and 1 s, respectively): (a) respiratory rate; (b) heartbeat rate.

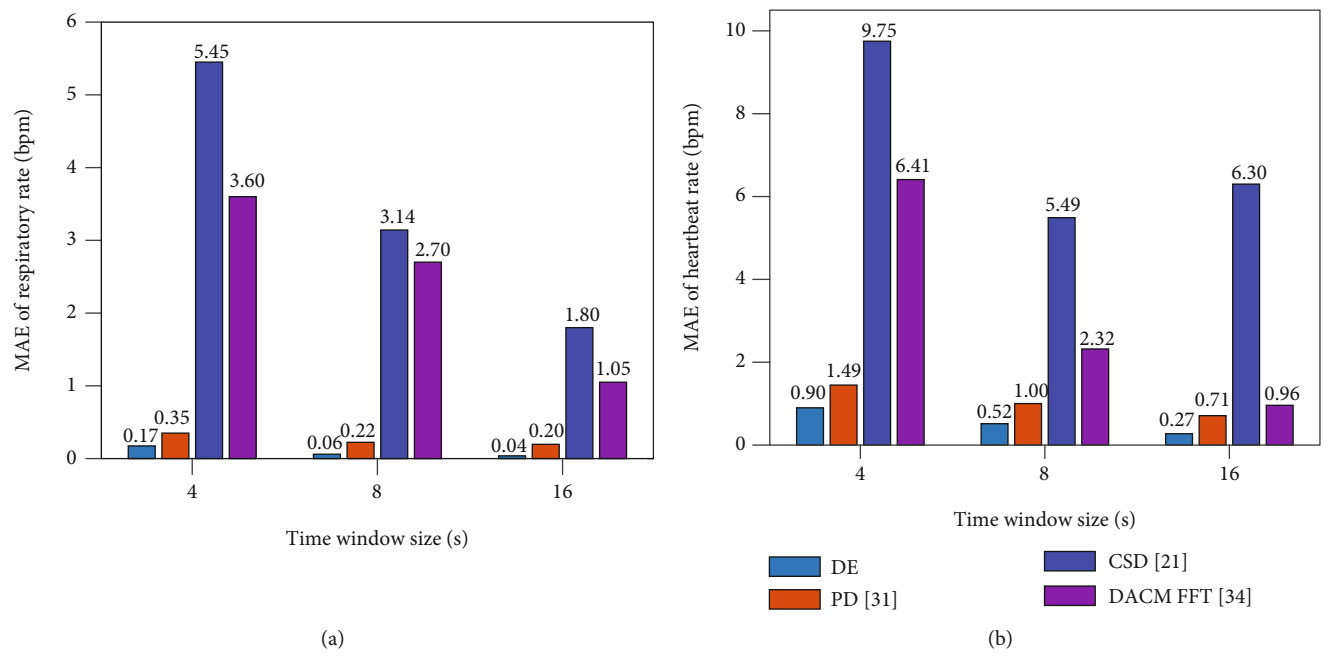

Figure 9: The mean absolute errors (MAE) of different time windows in controlled environment experiments: (a) the MAE of respiratory rate; (b) the MAE of heartbeat rate.

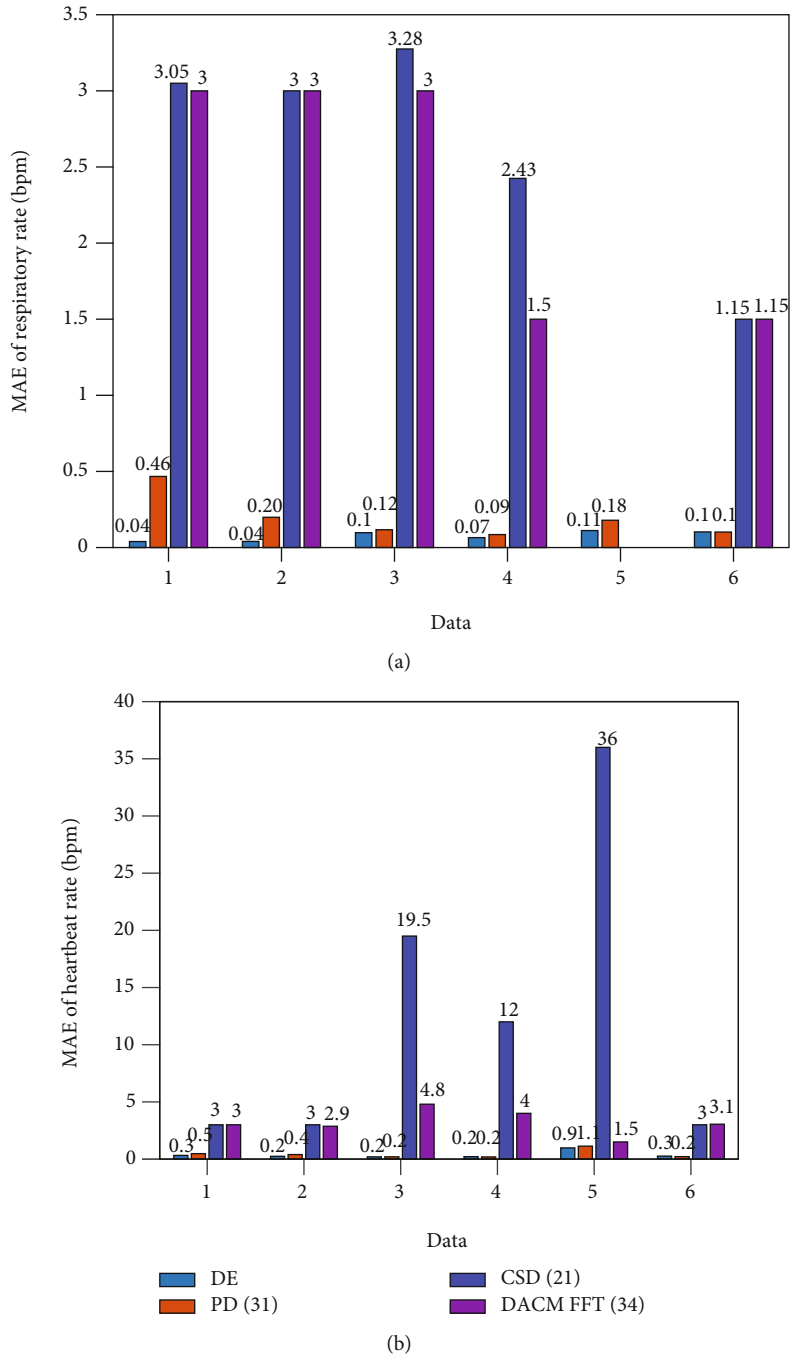

Figure 10: The mean absolute errors (MAE) under different amplitudes of respiration and heartbeat: (a) the MAE of respiratory rate; (b) the MAE of heartbeat rate.

In the digital field, the integration is replaced with accumulation. Hence, the displacement information $x(t)$ can be rewritten in the discrete form

$$x[n] = \sum_{k=2}^{n} \{\dot{x}[k]\Delta t]\} = \frac{\lambda}{4\pi} \sum_{k=2}^{n} \frac{I^c[n](Q^c[n] - Q^c[n-1]) - Q^c[n](I^c[n] - I^c[n-1])}{(A_Q/A_I)I^c[n]^2 + (A_I/A_Q)Q^c[n]^2}. \quad (7)$$

3. Respiratory and Heartbeat Parameter Extraction

The chest wall displacement $x(t)$ caused by respiration and heartbeat can be modeled as sinusoids with amplitudes m_r and m_h, frequencies f_r and f_h, and initial phases φ_r and φ_h [32].

$$x(t) = m_r \sin(2\pi f_r t + \varphi_r) + m_h \sin(2\pi f_h t + \varphi_h), \quad (8)$$

where subscripts r and h indicate the corresponding parameters of respiration and heartbeat, respectively. Instead of FFT [33], we directly estimate the frequencies by a swarm intelligence algorithm to reduce the size of time windows.

As the chest wall displacement $x(t)$ can be computed by Equation (7) from the calibrated I/Q signals, we can find the most matched parameters m_r, f_r, φ_r, m_h, f_h, and φ_h by solving

$$\min\left(\frac{1}{n}\sum_{i=1}^{n}|x(i)-m_r\sin(2\pi f_r t+\varphi_r)-m_h\sin(2\pi f_h t+\varphi_h)|\right), \tag{9}$$

where $x(i), i = 1, 2, \cdots, n$ represents the displacement calculated in the ith I/Q signals.

We choose the differential evolution algorithm [34] to solve this nonlinear optimization problem. The differential evolution algorithm shown in Figure 3 is a very simple yet fairly powerful stochastic global optimizer for continuous search domain. Practically, the parameters of respiration and heartbeat can be set up within a reasonable range for the purpose of improving the speed optimization and reducing the calculation amount. In this paper, the amplitude, frequency, and phase range of respiration and heartbeat are set between [0 mm 0.2 Hz $-\pi$ 0 mm 1 Hz $-\pi$] and [6 mm 0.8 Hz π 0.8 mm 2 Hz π]. As discussed in Section 4.3, the optimal population size and the number of iterations are set as 80 and 100, respectively.

To sum up, the proposed vital sign extraction method can be implemented with the following four steps.

(1) Collect the orthogonal output signals $I(t)$ and $Q(t)$ detected by Doppler radar

(2) Use the proposed correction method shown in Section 2.1 to remove phase imbalance, direct-current offsets, and gain error of I/Q signals

(3) Obtain the chest wall displacement information by the extended differentiate and cross multiply method shown in Section 2.2

(4) Estimate the parameters of respiration and heartbeat by the differential evolution algorithm

Figure 4 shows the comparison of the displacement extracted from radar outputs and the displacement reconstructed using the vital sign parameters estimated by the differential evolution algorithm. As can be seen from Figure 4, the reconstructed displacement is in good agreement with the reference, demonstrating the effectiveness of the proposed algorithm.

4. Experiments and Results

4.1. Experimental Setup and Methodology. To verify the effectiveness of the proposed algorithm, extensive experiments have been conducted in both controlled and real environments. Figure 5 shows the structure of the experimental setup. The amplified signals of radar are sampled by a microcontroller controlled 24 bit analog-to-digital converter with a sampling frequency of 50 Hz. The negative temperature coefficient (NTC) resistor installing in the breathing valve of mask provides the reference frequency of respiration by sensing the temperature change caused by exhaling hot airflow and inhaling cool airflow during respiration, and the pulse sensor provides the reference frequency of heartbeat by sensing the light transmittance change caused by heartbeat. Besides, the microcontroller also controls the movement of sliding table by using the stepper motor driver. All relevant data is sent to the PC via USB interface and processed by MATLAB R2018a.

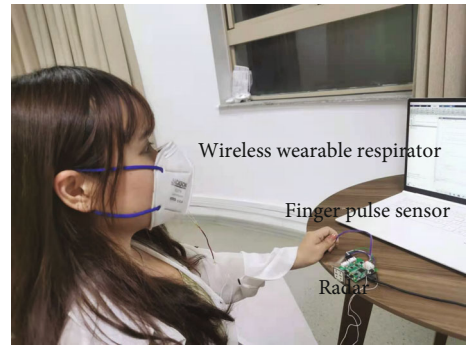

Figure 11: Experimental setup for vital sign detection.

We compare the proposed method with the complex signal demodulation method [21], the extended differentiate and cross multiply FFT method [27], and the parameterized demodulation method [32]. The complex signal demodulation method [21] combines the signals of I/Q channels into complex signals and performs spectrum analysis through FFT to obtain the frequencies of respiration and heartbeat. The extended differentiate and cross multiply FFT method [27] extracts displacement information from radar outputs and estimates frequencies using FFT. The parameterized demodulation method [32] defines a demodulation operator to obtain a high spectrum energy concentration and addresses the phase demodulation problem as a parameter optimization problem. Therefore, the frequency resolution problem can be avoided. In the following figures, we use CSD, DACM, and PD as abbreviations of the above methods.

4.2. Verification of I/Q Mismatch Correction. To verify the proposed correction method, we compare the estimated displacement from Equation (7) with the reference displacement of the object on the sliding table in the simulation setup. The amplitude and frequency of the slide movement are set to 0.5-3 mm and 0.3 Hz, respectively. Table 3 shows the mean absolute errors (MAE) of estimated displacement under different arc lengths. As the arc length of the ellipse decreases with the amplitude of movements, the estimation of ellipse parameters becomes difficult due to insufficient data incentive. As shown in Table 3, the performance of the least square-based ellipse fitting algorithm [29] is seriously affected by the reduction of arc length, while the

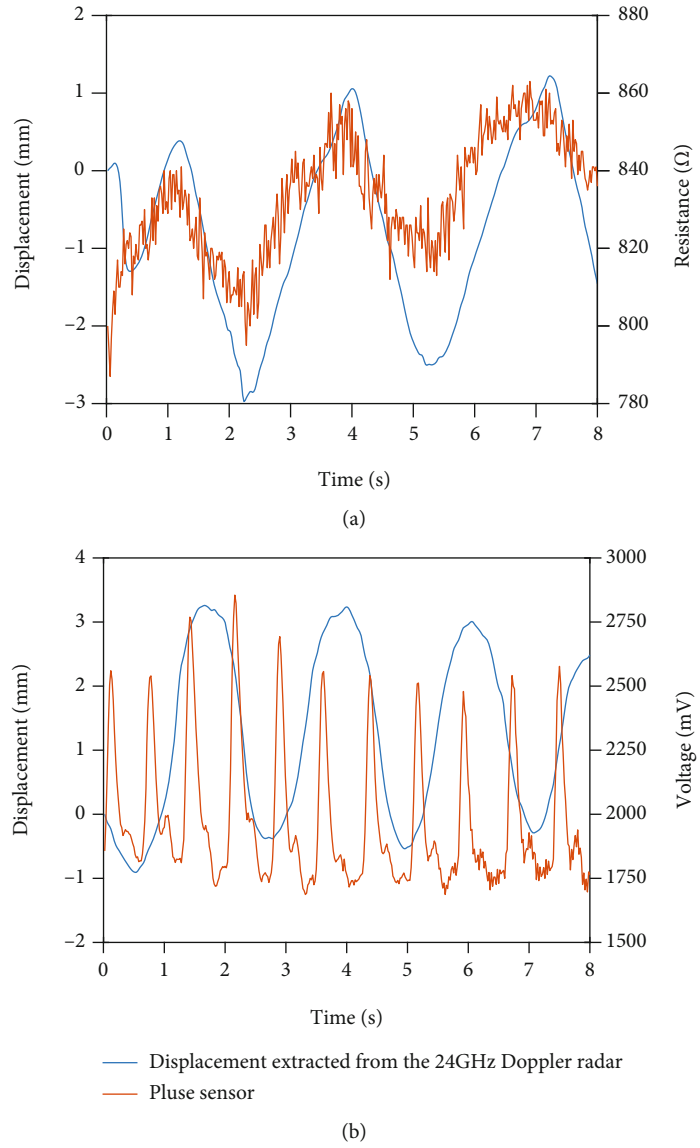

Figure 12: The chest wall displacement extracted from the 24 GHz Doppler radar and the reference signals: (a) the resistance change of the NTC resistor caused by respiration; (b) the voltage change of the pulse sensor caused by heartbeat.

proposed two-step correction algorithm is slightly affected. As shown in Figure 6, the proposed algorithm can accurately estimate the displacement of a moving object, even if the amplitude is 0.5 mm. However, the least square-based ellipse fitting algorithm [29] fails to estimate the displacement due to incorrect parameter estimation of an ellipse. The above results show that the proposed algorithm can accurately estimate the parameters of an ellipse with very short arc length and therefore is more suitable for the detection of slight breathing.

4.3. Determination of Differential Evolution Parameters. The population size and number of iterations are the key parameters affecting the accuracy and computational complexity of a differential evolution algorithm. A larger population size and a larger number of iterations help to reduce error but also increase computational complexity. Figure 7 shows the mean absolute errors (MAE) of estimated respiratory and heartbeat frequencies with different population sizes and numbers of iterations. It can be clearly seen that the errors decrease with the increase of population size and the number of iterations. Finally, the population size and the number of iterations are determined as 80 and 100, respectively, after which the downward gradients of errors have become very small.

4.4. Experiments in Controlled Environments. During the experiments in a controlled environment, the sliding table simulates the thoracic motion according to the movement mode given by Equation (8) and the parameters shown in Table 4. Figure 8 shows the estimated respiratory rate and heartbeat rate from data 3. The real respiratory and heartbeat frequencies are fixed at 18 bpm and 72 bpm, respectively. We then use a short time window of 16 s to increase

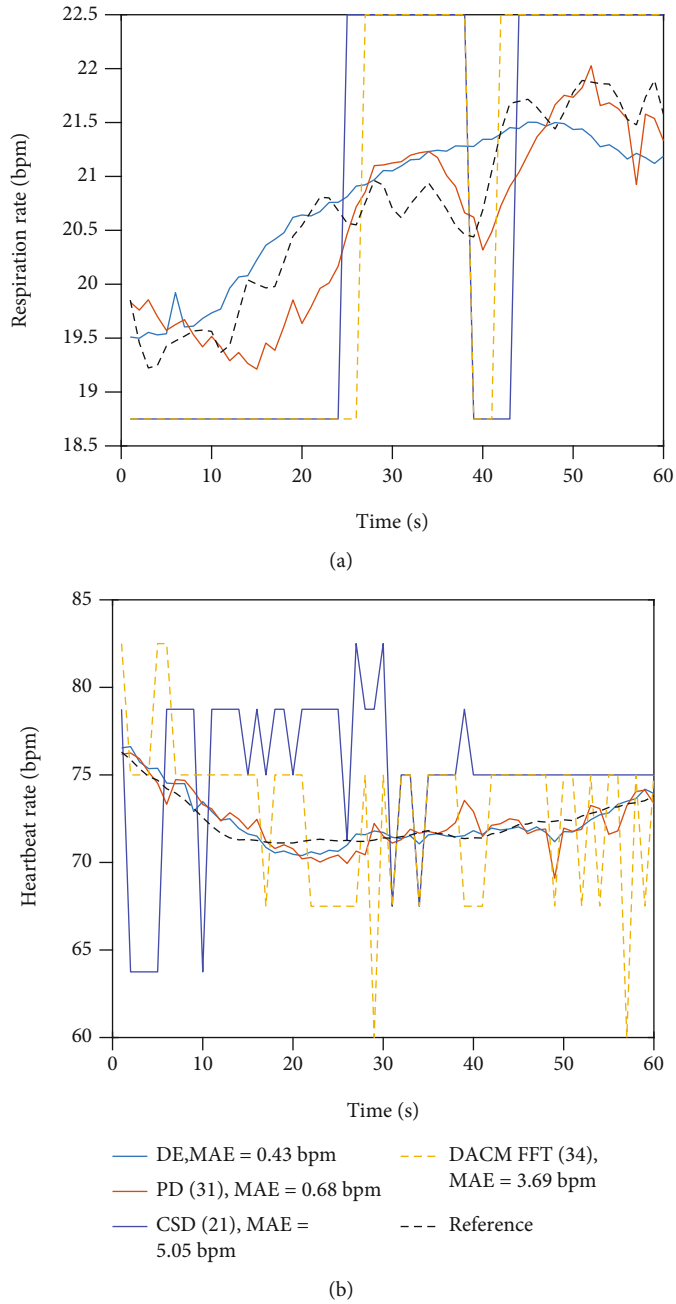

Figure 13: The extracted vital signs of different methods in real environments (the sliding window and the step size are 16 s and 1 s, respectively): (a) respiratory rate; (b) heartbeat rate.

the sensitivity. Since the frequency resolution of FFT is inversely proportional to the time window (1/16 s = 3.75 bpm), the respiratory and heartbeat frequencies estimated by the complex signal demodulation and the extended differentiate and cross multiply methods are 18.75 (5×3.75) bpm and 75 (20×3.75) bpm, respectively. Therefore, the estimation results of these two methods are far away from the real values. To improve measurement accuracy, the time window needs to be increased. But this reduces the real-time performance. While the frequency resolution of the parameterized demodulation method [32] and our proposed differential evolution (DE) method do not depend on the time window size, both methods can accurately extract the frequency information of respiration and heartbeat with a limited time window.

Figure 9 shows the influence of time window size on the mean absolute errors (MAE) of each method for data 1-6. Due to the large amplitude of chest motion caused by respiration, the estimated errors of respiratory rate are smaller than those of heartbeat rate. With the decrease of time window, the accuracy of FFT-based methods [21, 27] decreases dramatically. The parameterized demodulation method (PD) [32] and the proposed differential evolution method (DE) are only slightly affected. Our proposed

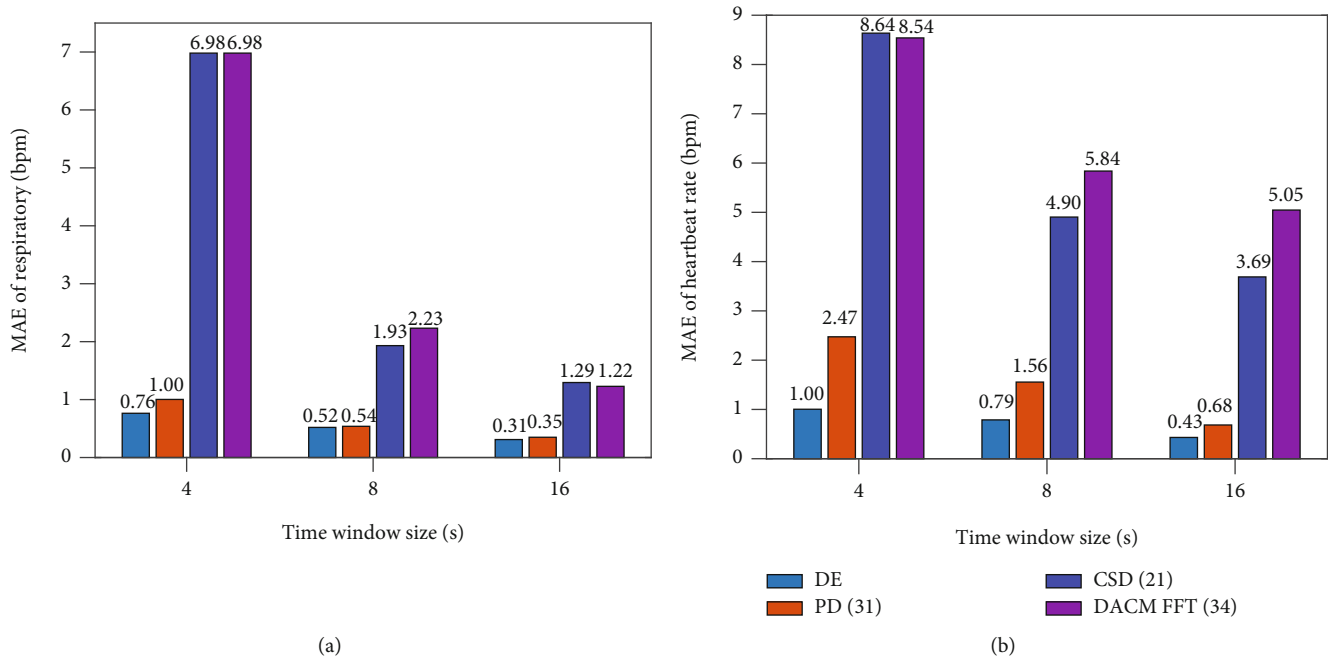

Figure 14: The mean absolute errors (MAE) of different time windows in real environment experiments: (a) the MAE of respiratory rate; (b) the MAE of heartbeat rate.

method performs better than the parameterized method on all time windows. Figure 10 shows the influence of amplitudes (m_r and m_h) on the MAE of each method. The time window is 8 s, corresponding to the frequency resolution of 7.5 bpm for FFT. Hence, for respiratory rate of 30 bpm, the respiratory errors of the FFT-based method [21, 27] are 0. As can be seen from Figure 10, the proposed differential evolution method is not affected by the amplitudes of respiration and heartbeat. Its MAEs of respiratory rate and heartbeat rate for $m_r = 1$ mm and $m_h = 0.1$ mm (data 1) are only 0.04 bpm and 0.32 bpm. As a comparison, the MAEs of parameterized demodulation method are 0.46 bpm and 0.48 bpm, respectively. Therefore, the proposed differential evolution method is more suitable for detecting slight breathing.

4.5. Experiments in Real Environments. As shown in Figure 11, during the experiments in real environments, a subject seated still in a chair and breathed naturally with her chest facing the antennas. At the same time, the subject wore the mask with NTC resistor and the finger pulse sensor shown in Figure 5 to measure the reference signals of respiration and heartbeat, respectively. Figure 12 shows the comparison between the signals measured by the NTC resistor, the pulse sensor, and the displacement demodulated from the 24 GHz Doppler radar. By performing peak-seeking operations on the above signals, the reference frequencies of respiration and heartbeat can be obtained.

Figure 13 shows the respiratory rate and the heartbeat rate obtained from the above vital sign extraction algorithms. The obtained parameters are estimated with data from a certain time window. A smaller time window can better reflect the changes in respiratory and heartbeat parameters and improve the real-time performance of the algorithm. In this paper, an overlapping sliding window with a window size of 16 s and a shift interval of 1 s was adopted to estimate the parameters. The total time length of the estimated parameters is 60 s. The reference is the average value of respiratory rate and heartbeat rate obtained in the time window of 16 s. It should be noted that the frequency resolution of FFT corresponding to the time window of 16 s is 3.75 bpm, which makes the results of the complex signal demodulation [21] and the extended differentiate and cross multiply methods [27] far away from the reference and fluctuate greatly. The parameterized demodulation algorithm [32] and the proposed differential evolution algorithm are not affected by the problem. The errors of the proposed differential evolution method (MAE = 0.31 bpm and 0.43 bpm for respiration and heartbeat) are smaller than those of parameterized demodulation method (MAE = 0.35 bpm and 0.68 bpm for respiration and heartbeat). As shown in Figure 14, the accuracy of the proposed differential evolution algorithm is also better than other algorithms in different time windows, especially in the case of short time window. These results show that the proposed differential evolution method is more suitable for real-time monitoring of vital signs in short time window.

5. Conclusions

In this paper, we proposed a novel vital sign signal extraction algorithm to accurately extract the respiratory and heartbeat parameters in short time window. The proposed method firstly corrects the I/Q signals according to the proposed two-step I/Q mismatch correction method. Then, the chest wall displacement can be obtained by the extended

differentiate and cross multiply method. Finally, the differential evolution method is used to estimate the parameters of respiration and heartbeat. The comprehensive experimental results demonstrate that the proposed method has higher accuracy than other existing vital sign extraction algorithms in Doppler radar vital sign detection, especially in the case of short time window. Our future work will focus on sleep stage detection based on these measured vital signs and machine learning.

Data Availability

The data used to support the findings of this study are available from the corresponding author upon request.

Conflicts of Interest

The authors declare that there is no conflict of interest regarding the publication of this paper.

Acknowledgments

This work was supported by the Zhejiang Provincial Natural Science Foundation of China under Grant No. LY19F010010.

References

[1] F. Zhang, C. Wu, B. Wang et al., "SMARS: sleep monitoring via ambient radio signals," *IEEE Transactions on Mobile Computing*, vol. 20, no. 1, pp. 217–231, 2021.

[2] H. Korkalainen, J. Aakko, S. Nikkonen et al., "Accurate deep learning-based sleep staging in a clinical population with suspected obstructive sleep apnea," *IEEE Journal of Biomedical and Health Informatics*, vol. 24, no. 7, pp. 2073–2081, 2020.

[3] H. Hong, L. Zhang, C. Gu, Y. Li, G. Zhou, and X. Zhu, "Noncontact sleep stage estimation using a CW Doppler radar," *IEEE Journal on Emerging and Selected Topics in Circuits and Systems*, vol. 8, no. 2, pp. 260–270, 2018.

[4] C. Lin, M. Prasad, C. Chung et al., "IoT-based wireless polysomnography intelligent system for sleep monitoring," *IEEE Access*, vol. 6, pp. 405–414, 2018.

[5] S. Milici, J. Lorenzo, A. Lazaro, R. Villarino, and D. Girbau, "Wireless breathing sensor based on wearable modulated frequency selective surface," *IEEE Sensors Journal*, vol. 17, no. 5, pp. 1285–1292, 2017.

[6] S. Milici, A. Lazaro, R. Villarino, D. Girbau, and M. Magnarosa, "Wireless wearable magnetometer-based sensor for sleep quality monitoring," *IEEE Sensors Journal*, vol. 18, no. 5, pp. 2145–2152, 2018.

[7] A. Siqueira, A. F. Spirandeli, R. Moraes, and V. Zarzoso, "Respiratory waveform estimation from multiple accelerometers: an optimal sensor number and placement analysis," *IEEE Journal of Biomedical and Health Informatics*, vol. 23, no. 4, pp. 1507–1515, 2019.

[8] F. Erden and A. E. Li, "Breathing detection based on the topological features of IR sensor and accelerometer signals," in *2016 50th Asilomar Conference on Signals, Systems and Computers*, pp. 1763–1767, Pacific Grove, CA, USA, 2016.

[9] H. Aly and M. Youssef, "Zephyr: ubiquitous accurate multi-sensor fusion-based respiratory rate estimation using smartphones," in *IEEE INFOCOM 2016 - The 35th Annual IEEE International Conference on Computer Communications*, pp. 1–9, San Francisco, CA, USA, 2016.

[10] D. Castaneda, A. Esparza, M. Ghamari, C. Soltanpur, and H. Nazeran, "A review on wearable photoplethysmography sensors and their potential future applications in health care," *International Journal of Biosensors Bioelectronics*, vol. 4, no. 4, pp. 195–202, 2018.

[11] O. Bertolli, S. Arridge, C. W. Stearns, S. D. Wollenweber, B. F. Hutton, and K. Thielemans, "Data driven respiratory signal detection in PET taking advantage of time-of-flight data," in *2016 IEEE Nuclear Science Symposium, Medical Imaging Conference and Room-Temperature Semiconductor Detector Workshop (NSS/MIC/RTSD)*, pp. 1–3, Strasbourg, France, 2016.

[12] R. Hostettler, O. Kaltiokallio, H. Yiğitler, S. Särkkä, and R. Jäntti, "RSS-based respiratory rate monitoring using periodic Gaussian processes and Kalman filtering," in *European Signal Processing Conference*, pp. 256–260, Kos, Greece, 2017.

[13] X. Liu, J. Cao, S. Tang, J. Wen, and P. Guo, "Contactless respiration monitoring via off-the-shelf WiFi devices," *IEEE Transactions on Mobile Computing*, vol. 15, no. 10, pp. 2466–2479, 2016.

[14] S. M. A. Tayaranian Hosseini, H. Amindavar, and M. Amirmazlaghani, "A new robust vital sign detection in complex environments using ultrawideband radar," *IEEE Transactions on Geoscience and Remote Sensing*, vol. 54, no. 11, pp. 6771–6782, 2016.

[15] W. Su, M. Tang, R. E. Arif, T. S. Horng, and F. K. Wang, "Stepped-frequency continuous-wave radar with self-injection-locking technology for monitoring multiple human vital signs," *IEEE Transactions on Microwave Theory and Techniques*, vol. 67, no. 12, pp. 5396–5405, 2019.

[16] G. Sun, T. Matsui, Y. Watai et al., "Vital-SCOPE: design and evaluation of a smart vital sign monitor for simultaneous measurement of pulse rate, respiratory rate, and body temperature for patient monitoring," *Journal of Sensors*, vol. 2018, no. 11, Article ID 4371872, 7 pages, 2018.

[17] L. Ren, L. Kong, F. Foroughian, H. Wang, P. Theilmann, and A. E. Fathy, "Comparison study of noncontact vital signs detection using a Doppler stepped-frequency continuous-wave radar and camera-based imaging photoplethysmography," *IEEE Transactions on Microwave Theory and Techniques*, vol. 65, no. 9, pp. 3519–3529, 2017.

[18] G. Wang, J. M. Munoz-Ferreras, C. Gu, C. Li, and R. Gomez-Garcia, "Application of linear-frequency-modulated continuous-wave (LFMCW) radars for tracking of vital signs," *IEEE Transactions on Microwave Theory and Techniques*, vol. 62, no. 6, pp. 1387–1399, 2014.

[19] M. Mercuri, Y. Liu, I. Lorato, T. Torfs, A. Bourdoux, and C. van Hoof, "Frequency-tracking CW Doppler radar solving small-angle approximation and null point issues in noncontact vital signs monitoring," *IEEE Transactions on Biomedical Circuits and Systems*, vol. 11, no. 3, pp. 671–680, 2017.

[20] W. Pan, J. Wang, J. Huangfu, C. Li, and L. Ran, "Null point elimination using RF phase shifter in continuous-wave Doppler radar system," *Electronics Letters*, vol. 47, no. 21, pp. 1196–1198, 2011.

[21] C. Li and J. Lin, "Complex signal demodulation and random body movement cancellation techniques for non-contact vital sign detection," in *International Microwave Symposium Digest*, pp. 567–570, Atlanta, GA, USA, 2008.

[22] K. Han and S. Hong, "Differential-phase radar with amplitude-compensated complex signal demodulation for vital sign

detection," in *Asia-Pacific Microwave Conference (APMC)*, pp. 1390–1392, Singapore, 2019.

[23] J. Tu and J. Lin, "Respiration harmonics cancellation for accurate heart rate measurement in non-contact vital sign detection," in *MTT-S International Microwave Symposium Digest (MTT)*, pp. 1–3, Seattle, WA, USA, 2013.

[24] B. Park, O. Boric-Lubecke, and V. M. Lubecke, "Arctangent demodulation with DC offset compensation in quadrature Doppler radar receiver systems," *IEEE Transactions on Microwave Theory and Techniques*, vol. 55, no. 5, pp. 1073–1079, 2007.

[25] W. Hu, Z. Zhao, Y. Wang, H. Zhang, and F. Lin, "Noncontact accurate measurement of cardiopulmonary activity using a compact quadrature Doppler radar sensor," *IEEE Transactions on Biomedical Engineering*, vol. 61, no. 3, pp. 725–735, 2014.

[26] J. Wang, X. Wang, L. Chen, J. Huangfu, C. Li, and L. Ran, "Noncontact distance and amplitude-independent vibration measurement based on an extended DACM algorithm," *IEEE Transactions on Instrumentation and Measurement*, vol. 63, no. 1, pp. 145–153, 2014.

[27] C. Gu, Y. He, and J. Zhu, "Noncontact vital sensing with a miniaturized 2.4 GHz circularly polarized Doppler radar," *IEEE Sensors Letters*, vol. 3, no. 7, pp. 1–4, 2019.

[28] Q. Lv, D. Ye, S. Qiao et al., "High dynamic-range motion imaging based on linearized Doppler radar sensor," *IEEE Transactions on Microwave Theory and Techniques*, vol. 62, no. 9, pp. 1837–1846, 2014.

[29] A. Singh, X. Gao, E. Yavari et al., "Data-based quadrature imbalance compensation for a CW Doppler radar system," *IEEE Transactions on Microwave Theory and Techniques*, vol. 61, no. 4, pp. 1718–1724, 2013.

[30] X. Gao, J. Xu, A. Rahman, V. Lubecke, and O. Boric-Lubecke, "Arc shifting method for small displacement measurement with quadrature CW doppler radar," in *2017 IEEE MTT-S International Microwave Symposium (IMS)*, pp. 1003–1006, Honololu, HI, USA, 2017.

[31] J. Park and J. Yang, "Multiphase continuous-wave Doppler radar with multiarc circle fitting algorithm for small periodic displacement measurement," *IEEE Transactions on Microwave Theory and Techniques*, pp. 1–1, 2020.

[32] Y. Xiong, S. Chen, X. Dong, Z. Peng, and W. Zhang, "Accurate measurement in Doppler radar vital sign detection based on parameterized demodulation," *IEEE Transactions on Microwave Theory and Techniques*, vol. 65, no. 11, pp. 4483–4492, 2017.

[33] M. H. Mostafa, S. Chamaani, and J. Sachs, "Singular spectrum analysis-based algorithm for vitality monitoring using M-sequence UWB sensor," *IEEE Sensors Journal*, vol. 20, no. 9, pp. 4787–4802, 2020.

[34] R. Storn and K. Price, "Differential evolution - a simple and efficient heuristic for global optimization over continuous spaces," *Journal of Global Optimization*, vol. 11, no. 4, pp. 341–359, 1997.